6th European Conference on Computational Mechanics (ECCM 6)
7th European Conference on Computational Fluid Dynamics (ECFD 7)
11 – 15 June 2018, Glasgow, UK

AN ENRICHED-FINITE ELEMENT TECHNIQUE FOR NUMERICAL SIMULATION OF HYDRO-FRACTURE EVOLUTION IN NATURALLY-LAYERED FORMATIONS

M. VAHAB[1], SH. AKHONDZADEH [2], A. R. KHOEI[3], AND N. KHALILI[4]

[1] UNSW
School of Civil and Environmental Engineering, the University of New South Wales, Sydney 2052, Australia.
m.vahab@unsw.edu.au

[2] Sharif University of Technology,
Center of Excellence in Structural and Earthquake Engineering, Department of Civil Engineering, Sharif University of Technology, P.O. Box. 11365-9313, Tehran, Iran.
akhondzadeh@gmail.com

[3] Sharif University of Technology,
Center of Excellence in Structural and Earthquake Engineering, Department of Civil Engineering, Sharif University of Technology, P.O. Box. 11365-9313, Tehran, Iran.
arkhoei@sharif.edu

[4] UNSW
School of Civil and Environmental Engineering, the University of New South Wales, Sydney 2052, Australia.
n.khalili@unsw.edu.au

Key words: Hydraulic fracture growth; X-FEM; layered domain; singular enrichment strategy.

Abstract. I*n this paper, a computational model is developed for the simulation of hydro-fracture growth in naturally layered impervious media using the extended finite element method (X-FEM). The equilibrium equation of the bulk is solved in conjunction with the hydro-fracture inflow and continuity equations using the staggered Newton method. The hydro-fracture inflow is modeled by using the lubrication theory, where the permeability of the fracture is incorporated by taking advantage of the cubic law. The Eigen-function expansion method is utilized in order to develop enrichment functions suited for the asymptotic stress field in the vicinity of the singular points. An energy release rate-based criterion is used in order to study the competition between hydro-fracture penetration/deflection at the material interface. Finally, the robustness of the computational framework is explored by means of numerical simulation.*

1 INTRODUCTION

Hydraulic fracturing (fracking) is a well-known engineering technique in which highly pressurized fluid injection is utilized in order to generate permeable fractures within low permeability formations. Fracking manifest in a wide range of engineering applications namely enhancing oil and gas recovery from tight reservoirs [1], block caving of mines [2], waste disposal and cleansing of contaminated soils [3], and geothermal energy production [4], to name a few. Geertsma and de'Klerk [5], Spence and Sharp [6], Khristianovic and Zheltov [7], and Hubbert and Willis [8] were amongst the first who proposed closed form analytical solutions to the problem of hydraulic fracturing. Early numerical simulations of fracking on the other hand were due to Daneshy [9], Haimson and Fairhurst [10], and Beach [11]. Many key features in modeling of hydraulic fracturing including hydro-mechanical coupling, matrix permeability, fluid-lag, and domain inhomogeneities were addressed in later contributions by Detournay and Cheng [1], Boone and Ingraffea [12], Secchi and Schrefler [13], Noorishad et al. [14], and Segura and Carol [15]. More recently, on the basis of the partition of unity concept, advanced numerical frameworks as such as X-FEM (e.g., Réthoré et al. [16], Khoei et al. [17], Vahab and Khalili [18, 19]), and mesh-free Galerkin methods (e.g., Oliaei et al. [20], Samimi and Pak [3]) are employed to more efficiently deal with the computationally complex problem of fracking.

Geological formations generally contain inhomogeneities, which can significantly affect their geomechanical characteristics. Thiercelin et al. [21] studied hydro-fractures approaching material interfaces within domains subjected to traction-free boundaries, and showed hydro-fractures can penetrate across such interfaces regardless of material properties. Eekelen [22] investigations indicated neither contrast in stiffness nor in-situ stresses can prevent hydraulic fracture penetration into the surrounding layers. On the contrary, Biot et al. [23] implied unless a critical fluid pressure is exceeded any mechanical property differences may cease fracture penetration. Using a stress analysis, Gudmundsson and Brenner [24] concluded that hydro-fractures penetrate material interfaces merely in soft to stiff configuration due to stress built up within the secondary domain. In contradiction, Wang [25] analysis showed that hydro-fractures tend to propagate into softer rocks which require less fracture energy and driving force. Behnia et al. [26] performed an energy analysis to show that even minor inclination angle may lead to rapid diversion of the hydro-fracture from the interface in soft to stiff configuration.

The hydro-fracture interaction with material interfaces is indeed an open area of research and the literature has not yet reached a consensus. The aim of this paper is to develop a rigorous energy based numerical framework so as to explore the penetration/deflection of the hydro-fracture at material interfaces. The penetration/deflection criterion introduced by Ming-Yuan and Hutchinson [27] and Hutchinson and Sue [28] is employed, in which admissible interaction scenario is determined through the elaboration of the second law of thermodynamics in conjunction with the minimization of the total potential energy. To this end, the interfacial fracture toughness is computed using the mode mixity parameter, which is in turn a function of the Stress Intensity Factors (SIFs) associated with the fracture tip merged with the material interface. The stress singularity in the vicinity of crack-tips is captured by taking advantages from the recent X-FEM developments by Akhondzadeh et al. [29], which ensures the high resolution of the stress field as well as the precision and reliability of the

model simulations. Finally, the robustness of the proposed computational framework is examined through numerical simulation.

2 PROBLEM DEFINITION

Consider a two-dimensional impermeable domain Ω bounded by the external boundary Γ, with the external normal unit vector $\mathbf{n}_\Gamma$ (see **Figure 1**). The external boundary conditions are defined as the prescribed traction $\mathbf{t}$ and the prescribed displacement $\bar{\mathbf{u}}$ which are respectively imposed on Γ_t and Γ_u, such that $\Gamma_t \bigcup \Gamma_u = \Gamma$ and $\Gamma_t \bigcap \Gamma_u = \varnothing$ hold. The domain is composed of two subdomains Ω_i $(i = 1, 2)$, which are fully bonded at the intersection of two subdomains indicated by $\Gamma_{\mathcal{M}}$ and the normal unit vector $\mathbf{n}_{\Gamma_{\mathcal{M}}}$. An internal hydro-fracture interface $\Gamma_{\mathcal{HF}}$ is assumed with the unit normal vector $\mathbf{n}_{\Gamma_{\mathcal{HF}}}$, which is subjected to the fracturing fluid injection $\mathcal{Q}_{\mathcal{INJ}}$ that induces the fluid pressure $\boldsymbol{p}^{\mathcal{HF}} = p\,\mathbf{n}_{\Gamma_{\mathcal{HF}}}$. The contact tractions $\mathbf{t}^{\mathcal{Cont}}$ are defined on the basis of contact constitutive relations, which are activated so as to prevent the overlap of the fracture faces. The fractured domain is governed by the linear momentum balance equation, which can be expressed in quasi-static condition by assuming infinitesimal deformations as

$$\nabla \cdot \boldsymbol{\sigma} + \rho \mathbf{b} = \mathbf{0}, \tag{1}$$

where ρ is the bulk density, $\mathbf{b}$ is the body force per unit mass vector, and $\boldsymbol{\sigma}$ is the Cauchy stress tensor described as $\boldsymbol{\sigma} = \mathbf{D} : \boldsymbol{\varepsilon}$, with $\boldsymbol{\varepsilon}(\mathbf{u}) = \nabla^s \mathbf{u}$. The weak form of the momentum balance equation (1) is derived through the introduction of the test and trial functions of the dispalcement field $\mathscr{U}$ and $\delta\mathscr{U}$, respectively, as

$$\delta\Pi^{domain} = \int_\Omega \delta\boldsymbol{\varepsilon} : \boldsymbol{\sigma}\, d\Omega + \int_{\Gamma_{\mathcal{HF}}} [\![\delta\mathbf{u}]\!] \cdot p\,\mathbf{n}_{\Gamma_{\mathcal{HF}}}\, d\Gamma - \int_\Omega \delta\mathbf{u} \cdot \rho\mathbf{b}\, d\Omega - \int_\Gamma \delta\mathbf{u} \cdot \mathbf{t}\, d\Gamma = 0, \tag{2}$$

where the notation $[\![*]\!]$ is defined as $[\![*]\!] = *^+ - *^-$.

The hydro-fracture inflow on the other hand is governed by means of flow continuity equations. Using the local Cartesian coordinate system (x', y'), in which x' and y' are aligned with the tangent and normal to the flow line, and assuming a one-dimensional incompressible Newtonian flow for the fracturing fluid within the cavity, the continuity equation is expressed as

$$\frac{\partial \mathcal{Q}}{\partial x'} + [\![\dot{u}_{\mathrm{N}}]\!] + \mathcal{Q}' = 0, \tag{3}$$

where $\mathcal{Q}$ is the flow rate, $\mathcal{Q}'$ is the leak-off flow given by Carter's relation [30], and $[\![u_{\mathrm{N}}]\!]$ is the normal component of the relative jump in displacement field (crack opening) with over-dot indicating the time derivative. The hydro-fracture inflow is described by using the cubic law as

$$\mathcal{Q} = \frac{1}{f}\frac{h^3}{12\mu}\frac{\partial p}{\partial x'} \equiv \kappa_{\Gamma_{\mathcal{HF}}} \cdot \frac{\partial p}{\partial x'} . \tag{4}$$

In the above relation, $h = [\![u_{\mathrm{N}}]\!]$ is the hydro-fracture opening, μ is the fluid viscosity, and f is the modification factor suggested by Witherspoon et al. [31] which accounts for the deviations from the ideal condition of the parallel smooth crack faces.

Contact tractions $\mathbf{t}^{\mathcal{C}ent}$ are computed versus the normal and tangential gap vectors $\mathcal{G}_{\mathrm{N}}$ and $\mathcal{G}_{\mathrm{T}}$ described as

$$\begin{aligned} \mathcal{G}_{\mathrm{N}} &= (\mathbf{n}_{\Gamma_{\mathcal{HF}}} \otimes \mathbf{n}_{\Gamma_{\mathcal{HF}}})[\![\mathbf{u}]\!] \qquad \text{on } \mathbf{n}_{\Gamma_{\mathcal{HF}}}, \\ \mathcal{G}_{\mathrm{T}} &= (\mathbf{I} - \mathbf{n}_{\Gamma_{\mathcal{HF}}} \otimes \mathbf{n}_{\Gamma_{\mathcal{HF}}})[\![\mathbf{u}]\!] \qquad \text{on } \mathbf{n}_{\Gamma_{\mathcal{HF}}}, \end{aligned} \tag{5}$$

where $\mathbf{n}_{\Gamma_{\mathcal{HF}}} \otimes \mathbf{n}_{\Gamma_{\mathcal{HF}}}$ is the normal projection tensor. The first Kuhn-Tucker constraints in normal direction can be expressed as

$$\mathcal{G}_{\mathrm{N}} \geq 0, \quad t_{\mathrm{N}}^{\mathcal{C}ent} \leq 0, \quad \mathcal{G}_{\mathrm{N}}\, t_{\mathrm{N}}^{\mathcal{C}ent} = 0 \qquad \forall \boldsymbol{x} \in \Gamma_{\mathcal{HF}}, \tag{6}$$

where $t_{\mathrm{N}}^{\mathcal{C}ent}$ is the normal component of the contact tractions defined as $t_{\mathrm{N}}^{\mathcal{C}ent} = \mathbf{t}^{\mathcal{C}ent}.\mathbf{n}_{\Gamma_{\mathcal{HF}}}$, and $\mathcal{G}_{\mathrm{N}}$ is the normal gap defined as $\mathcal{G}_{\mathrm{N}} = \|\mathcal{G}_{\mathrm{N}}\|$. The normal component of the contact tractions are related to the normal penetration of the contacting surfaces through the application of a normal penalty parameter k_N as $\mathbf{t}_{\mathrm{N}}^{\mathcal{C}ent} = k_N\, \mathcal{G}_{\mathrm{N}}$. In the tangential direction on the other hand the contact tractions are defined as $\mathbf{t}_{\mathrm{T}}^{\mathcal{C}ent} = k_{\mathrm{T}}\, \mathcal{G}_{\mathrm{T}}$ (for stick condition), yet it obeys the slip criterion defined by the standard Coulomb's friction law as

$$\mathcal{F}_f = \left\|\mathbf{t}_T^{\mathcal{C}ent}\right\| - (c_f + \mu_f . t_N^{\mathcal{C}ent}) \begin{cases} < 0 & \text{Stick}, \\ = 0 & \text{Slip}, \end{cases} \tag{7}$$

where c_f and μ_f are the Coulomb's cohesion and friction coefficients, respectively. The tangential stick/slip condition is governed by the second Kuhn-Tucker relation expressed as

$$d\lambda \geq 0, \qquad \mathcal{F}_f \leq 0, \qquad d\lambda . \mathcal{F}_f = 0, \tag{8}$$

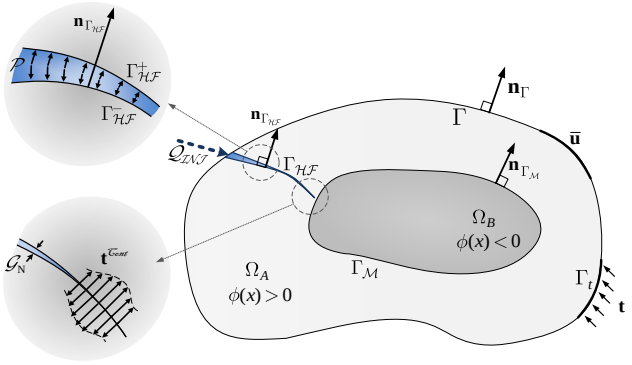

Figure 1 Hydro-fracture subjected to layered domain; problem definition and boundary conditions.

where $d\lambda = |d\mathcal{G}_{\mathrm{T}}|$ is the magnitude of the sliding increment.

3 DISCRETIZATION

The extended finite element method is elaborated in order to discretize the weak form of the equilibrium equation of the fractured domain given by equation (2). The X-FEM approximation of the displacement field $\mathbf{u}^h(\boldsymbol{x},t)$ is expressed as

$$\mathbf{u}^h(\boldsymbol{x},t) = \mathbf{u}^{\mathrm{std}}(\boldsymbol{x},t) + \mathbf{u}^{\mathcal{HF}}(\boldsymbol{x},t) + \mathbf{u}^{\mathcal{M}}(\boldsymbol{x},t)\,, \tag{9}$$

in which $\mathbf{u}^{\mathrm{std}}$, $\mathbf{u}^{\mathcal{HF}}$ and $\mathbf{u}^{\mathcal{M}}$ are associated with the standard, hydro-fracture and bimaterial displacement field, respectively, that can be expressed as

$$\mathbf{u}^{\mathrm{std}} = \sum_{I\in\mathcal{N}^{\mathrm{std}}} N_I(\boldsymbol{x})\mathbf{u}_I(t) \tag{10-a}$$

$$\begin{aligned}\mathbf{u}^{\mathcal{HF}}(\boldsymbol{x},t) = &\sum_{I\in\mathcal{M}^{\mathrm{Hev}}} N_I(\boldsymbol{x})\;\; \mathcal{H}(\phi_{\Gamma_{\mathcal{HF}}}(\boldsymbol{x})) - \mathcal{H}(\phi_{\Gamma_{\mathcal{HF}}}(\boldsymbol{x}_I))\;\; \bar{\mathbf{a}}_I \\ &+ \sum_{I\in\mathcal{M}^{\mathrm{Tip}}} N_I(\boldsymbol{x}) \sum_{\alpha=1}^{\mathcal{M}} \mathcal{B}^{\alpha}(\boldsymbol{x}) - \mathcal{B}^{\alpha}(\boldsymbol{x}_I)\;\; \mathcal{R}_{\mathrm{Tip}}(\boldsymbol{x})\,\bar{\mathbf{b}}_{\alpha I}\,,\end{aligned} \tag{10-b}$$

$$\mathbf{u}^{\mathcal{M}}(\boldsymbol{x},t) = \sum_{I\in\mathcal{M}^{\mathrm{Ridge}}} N_I(\boldsymbol{x})\mathcal{D}_m(\phi_{\Gamma_{\mathcal{M}}}(\boldsymbol{x}))\bar{\mathbf{c}}_I\,. \tag{10-c}$$

In the above relation, N_I is the standard shape function of node I corresponding to the standard DOFs $\mathbf{u}_I(t)$, and $\mathcal{N}^{\mathrm{std}}$ is the set of nodal points consisting the whole domain. Moreover, $\mathcal{H}$ and $\mathcal{B}^{\alpha}$ are the Heaviside and asymptotic enrichment functions, respectively, with $\bar{\mathbf{a}}_I$ and $\bar{\mathbf{b}}_{\alpha I}$ being the DOFs associated with the Heaviside and asymptotic parts of the displacement field. Finally, $\mathcal{D}_m(\boldsymbol{x})$ is the ridge enrichment function, with $\bar{\mathbf{c}}_I$ denoting the DOFs corresponding to the ridge parts of the displacement field. Notably, the asymptotic enrichment functions for fracture tips terminated at material interface must be replaced by incorporating the terms manifest in the Airy stress function solution of the displacement field as (see Bouhala et al. [32]):

$$\begin{aligned}\mathcal{B}^{\mathrm{SSE}}_{\mathrm{Tip}}(r,\theta) &= \left\{\mathcal{B}_1,\mathcal{B}_2,\mathcal{B}_3,\mathcal{B}_4\right\} \qquad\qquad \text{for } \theta_c = \pi/2 \\ &= \left\{r^{\lambda}\sin\big((\lambda\pm1)\theta\big),\; r^{\lambda}\cos\big((\lambda\pm1)\theta\big)\right\}, \\ \mathcal{B}^{\mathrm{SSE}}_{\mathrm{Tip}}(r,\theta) &= \left\{\mathcal{B}_1,\mathcal{B}_2,...,\mathcal{B}_8\right\} \qquad\qquad \text{for } \theta_c > \theta_p \\ &= \left\{r^{\lambda_j}\sin\big((\lambda_j\pm1)\theta\big),\; r^{\lambda j}\cos\big((\lambda_j\pm1)\theta\big)\right\},\quad j=1,2\end{aligned} \tag{11}$$

$$\mathcal{B}_{\text{Tip}}^{\text{SSE}}(r,\theta)=\left\{\mathcal{B}_1,\mathcal{B}_2,...,\mathcal{B}_{16}\right\} \qquad \text{for}\,\theta_c<\theta_p$$

$$=\Big\{r^{\lambda_{\text{Re}}}e^{\pm\lambda_{\text{Im}}\theta}\cos\big(\lambda_{\text{Im}}\ln(r)\big)\cos\big((\lambda_{\text{Re}}\pm1)\theta\big),\;\; r^{\lambda_{\text{Re}}}e^{\pm\lambda_{\text{Im}}\theta}\cos\big(\lambda_{\text{Im}}\ln(r)\big)\sin\big((\lambda_{\text{Re}}\pm1)\theta\big),$$

$$r^{\lambda_{\text{Re}}}e^{\pm\lambda_{\text{Im}}\theta}\sin\big(\lambda_{\text{Im}}\ln(r)\big)\cos((\lambda_{\text{Re}}\pm1)\theta),\;\; r^{\lambda_{\text{Re}}}e^{\pm\lambda_{\text{Im}}\theta}\sin\big(\lambda_{\text{Im}}\ln(r)\big)\sin\big((\lambda_{\text{Re}}\pm1)\theta\big)\Big\},$$

in which θ_p is the power logarithmic angle defined as the angle where the transition between real and imaginary solutions for λ occur. The singular enrichment function used in this work for the instance of crack terminating at the material interface is the modified version of the above enrichment functions, in which a weighted summation of the above functions, on the basis of the the Airy stress function coefficients is employed as the enrichment function. This approach, known as the modified singular enrichments (MSE), reduce the number of enrichment functions with increased accuracy (see Akhondzadeh et al. [29]).

The finite difference method is utilized in order to solve the flow continuity equations (3) and (4). Adopting the first-order upwind scheme for the spatial discretization of the fluid pressure field p and the flow rate $\mathcal{Q}$ it follows that (see [33])

$$\frac{\partial \mathcal{Q}_n^{\,j+1}}{\partial x'_n}=\frac{\mathcal{Q}_n^{\,j+1}-\mathcal{Q}_n^{\,j}}{\Delta x_n'^{\,j}}\,, \tag{12-a}$$

$$\frac{\partial p_n^{\,j+1}}{\partial x'_n}=\frac{p_n^{\,j+1}-p_n^{\,j}}{\Delta x_n'^{\,j}}, \tag{12-b}$$

where j stands for the $(j)^{th}$ discretization point of the FD solution. The time derivative of the hydro-fracture opening in direction normal to the fracture (i.e., $\dot{u}_{\text{N}}$) is approximated between two sequential time steps n and $n+1$ using the first-order upwind scheme as

$$[\![\dot{u}_{\text{N}}]\!]_{n+1}^{j}=\frac{[\![u_{\text{N}}]\!]_{n+1}^{j}-[\![u_{\text{N}}]\!]_{n}^{j}}{\Delta t}, \tag{13}$$

where the time increment is defined as $\Delta t=t_{n+1}-t_n$.

4 THE PENETRATION/DEFLECTION CRITERION

Based on the literature (e.g. see Martinez and Gupta [34]), the interaction of hydro-fractures with material interfaces leads to three distinct scenarios; hydro-fracture may penetrate across the interface, as the successful scenario, or it can be deflected either along one or both wings of the interface, which is referred to as failure. The resulting interaction scenario is determined by taking advantages from the energy release rate associated with each scenario. Based on Hutchinson and Suo [28], the singly deflected case is always energetically favorable in comparison to the doubly deflected case. Accordingly, the doubly deflected case is disregarded in the present study. The penetration/ deflection criterion is defined based on Ming-Yuan and Hutchinson [27] as

$$\begin{cases} \dfrac{\mathcal{G}_d}{\mathcal{G}_p^{\max}} < \dfrac{\mathcal{G}_{\text{intf}}}{\mathcal{G}_2} & \text{penetration,} \\ \dfrac{\mathcal{G}_d}{\mathcal{G}_p^{\max}} > \dfrac{\mathcal{G}_{\text{intf}}}{\mathcal{G}_2} & \text{deflection.} \end{cases} \tag{14}$$

In the above relations, $\mathcal{G}_2$ and $\mathcal{G}_{intf}$ are the fracture toughness of the secondary material and the interface, respectively, and $\mathcal{G}_p^{\max}$ is the penetration energy release rate which is determined as the maximum value of the energy release rate related to the penetrated crack at all plausible penetration angles. Based on Hutchinson and Suo [28], and Banks-Sills and Ashkenazi [35] the interfacial fracture toughness associated with a bimaterial interface intersected by a fracture is estimated by

$$\mathcal{G}_{\text{intf}} = \hat{\mathcal{G}}(1+\tan^2\Psi), \tag{15}$$

in which $\hat{\mathcal{G}}$ is the reference energy release rate, and Ψ is the mode mixity which is defined as

$$\Psi = \tan^{-1}\left(\frac{\mathcal{K}_{II}^{\text{intf}}}{\mathcal{K}_{I}^{\text{intf}}}\right). \tag{16}$$

Due to difference in the order of singularities due to appearance of λ_1 and λ_2 in the generalized SIFs (i.e., $\mathcal{K}_I^{\text{intf}}$ and $\mathcal{K}_{II}^{\text{intf}}$), they do not contain the identical units. Thus, a characteristic length factor of $l_0^{\lambda_1-\lambda_2}$ is applied to the nominator of the above relation so that the units be compatible.

The deflection energy release rate $\mathcal{G}_d$ is calculated by adopting the values of the SIFs obtained via the solution of an imaginary debounding of the material interface with an arbitrary length occurring in a single side as

$$\mathcal{G}_d = \frac{\eta[(\mathcal{K}_I^d)^2 + (\mathcal{K}_{II}^d)^2]}{E_1}, \tag{17}$$

where η is a coefficient depending on the material properties on either sides of the interface (see Vahab et al. [36]).

Finally, $\mathcal{G}_p^{\max}$ is computed through the auxiliary solution of the imaginary hydro-fracture penetration at the bimaterial interface using the same arbitrary growth length used in the singly deflected case as $\mathcal{G}_p = [(\mathcal{K}_I^p)^2 + (\mathcal{K}_{II}^p)^2]/E_2$.

5 NUMERICAL SIMULATION RESULTS

Numerical simulations here are performed by using an impervious $8\text{m}\times 8\text{m}$ rock block under plane strain condition. Four different material configurations are assumed for the block categorized into: 1) soft to stiff ($E_1 = E_0, E_2 = 2E_0$ or $4E_0, \nu_1 = \nu_2 = \nu_0$), and 2) stiff to soft (

$E_1 = 2E_0$ or $4E_0, E_2 = E_0, \nu_1 = \nu_2 = \nu_0$), with $E_0 = 10$ GPa and $\nu_0 = 0.3$ respectively being the reference Young modulus of elasticity and Poisson's ratio. A hydro-fracture of negligible length is positioned at the left surface of the block with initial inclination angles of $\theta_i = 0°, 15°$ and $30°$. The hydro-fracture is permitted to evolve from the right tip until it merges with the material interface located at $x = 4\,\text{m}$. The fracturing fluid is injected at the constant rate of $\mathcal{Q}_{INJ} = 10^{-3}\,\text{m}^2/\text{s}$ with the dynamic fluid viscosity of $\mu = 0.001$ Pa.s (see **Figure 2**). To prevent the overlap of the fracture edges, the contact parameters are set to $k_N = 10^6\,\text{MPa/mm}$. For all cases the fracture toughness of the secondary domain, $\mathcal{G}_2$, is set to $100\ \text{J}/\text{m}^2$. The interfacial toughness on the other hand is computed by setting $\hat{\mathcal{G}} = 50\ \text{J}/\text{m}^2$, in conjunction with a characteristic length of $\ell_0 = 0.4\,\text{m}$. Finally, the possibility of the occurrence of deflection or penetration scenario in each case is determined by introduction of the deflection and penetration factors defined as $\mathcal{R}_1 = \mathcal{G}_d / \mathcal{G}_{\text{intf}}$ and $\mathcal{R}_2 = \mathcal{G}_p^{\max} / \mathcal{G}_2$, respectively.

5.1 The soft to stiff configuration

The deflection energy release rate and deflection factor $\mathcal{G}_d$ and $\mathcal{R}_1$ are calculated based on the values of $\mathcal{K}_I^d$ and $\mathcal{K}_{II}^d$, where all the final values are given in **Table 1**. The penetration energy release rate on the other hand is calculated using the same crack increment (i.e., $\ell_0 = 0.4\,\text{m}$). The maximum penetration energy release rate associated with each case is utilized in order to determine the governing penetration factor, $\mathcal{R}_2$. As can be seen, in the case of $E_2 / E_1 = 2$ the penetration factors related to $\theta_i = 0°, 15°$ is slightly higher than the corresponding deflection factors; hence, for these cases the penetration scenario is more probable. However, by increasing the initial inclination angle to $\theta_i = 30°$ the deflection scenario predominates. Interestingly, by increase in stiffness contrast from 2 to 4 the penetration factors are significantly decreased. This is justified by taking into account that the energy release rate is reversely proportional to the material stiffness. Results here clearly imply that the hydro-fracture is highly prone to be deflected at the material interfaces in soft to stiff configuration.

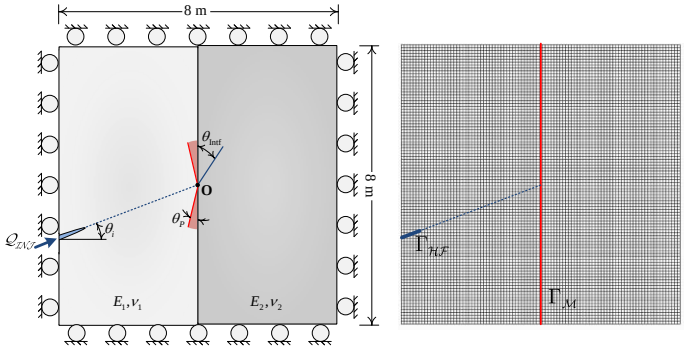

Figure 2 Hydro-fracture evolution throughout a bimaterial block; the problem definition, boundary conditions and FE mesh.

5.2 The stiff to soft configuration

In **Table 2**, the values of the SIFs $\mathcal{K}_I^d$ and $\mathcal{K}_{II}^d$, deflection energy release rate $\mathcal{G}_d$, deflection factor $\mathcal{R}_1$, and the maximum penetration energy release rate $\mathcal{R}_2$ are reported. Notably, the values of the deflection factors are only slightly increased in comparison to the first example; yet, the penetration factors are significantly increased. This can be justified due to the intensified stress field within the primary domain on one hand, and the appearance of the lower Young modulus in calculation of the energy release rate within the secondary domain ($\mathcal{G}_P \propto 1/E_2$) on the other hand. Therefore, in contrast to the first example, for all cases the penetration scenario is observed. Based on the results obtained in here, by increasing the stiffness contrast the penetration factors grow much faster than the deflection factors, which in turn leads to the increase in the probability of the penetration scenario. Hence, it can be concluded that for the material configuration of stiff to soft the probability of hydro-fracture penetration is higher in general.

6 CONCLUSIONS

In the present paper, an extended finite element framework is employed to simulate hydraulic fracturing within layered domains. The viscous fluid flow within the hydro-fracture is modelled by using the lubrication theory in which the fracture permeability is determined based on the cubic law. Contact along the fracture edges is implemented by using the X-FEM Penalty approach. Exploiting the enrichment strategy, the discretization of the displacement field is performed. In this regard, the asymptotic fields around the singular points are modeled by taking advantages from the Eigen-function expansion method which gives a high resolution to the stress field. The well-known penetration/deflection criterion introduced by Ming-Yuan and Hutchinson [27] is utilized in order to predict the plausible penetration/deflection scenario throughout the interaction of hydro-fractures with material interfaces. Finally, the performance of the developed framework is explored by means of numerical simulation. In the first example, the effects of soft to stiff configuration of the material interfaces as well as the role of initial inclination of perforations are investigated. Based on the energy analysis performed, it is shown that by increase in either the stiffness contrast or the initial inclination angle the probability of hydro-fracture deflection at the material interface dramatically increases. The second example studies the interaction of hydro-fractures with stiff to soft configured material interfaces. Taking into account that the penetration factors are substantially greater than their corresponding deflection factors, it is concluded that in general for stiff to soft configurations of material interfaces the probability of hydro-fracture penetration is quite high. The results suggested in the current study are believed to give a better understanding from the interaction problem for being based on a higher resolution for the stress field on one hand, and the use of the penetration/deflection criterion which is based on energy analysis on the other hand.

REFERENCES

[1] Detournay, E. and Cheng, A.H.D. Fundamentals of poroelasticity. *Compr. Rock. Eng. Princ. Pract. Proj.* (1995) **2**:113-171.

Table 1 Values of the penetration/deflection parameters for hydro-fracture subjected to bimaterial interface for soft to stiff configuration;

$E_2 / E_1 = 2$													
θ_i	$\mathcal{K}_I^{\text{intf}}$	$\mathcal{K}_{II}^{\text{intf}}$	Ψ	$\mathcal{G}_{\text{intf}}$	$\mathcal{K}_I^d$	$\mathcal{K}_{II}^d$	$\mathcal{G}_d$	$\mathcal{R}_1^*$	$\mathcal{K}_I^p$	$\mathcal{K}_{II}^p$	$\mathcal{G}_p^{\max}$	$\mathcal{R}_2^*$	Scenario
0°	2.24E+05	-1.67E+03	-0.007	50.0	2.13E+04	-7.57E+04	2.91E+00	0.0580	3.59E+05	-1.36E-01	5.877	0.0588	P
15°	5.09E+05	3.32E+05	0.594	72.8	2.73E+04	8.43E+04	3.70E+00	0.0508	3.79E+05	-1.91E+03	6.553	0.0655	P
30°	6.53E+05	2.99E+05	0.455	62.0	1.83E+04	-1.20E+05	6.92E+00	0.1120	3.92E+05	1.56E+05	9.623	0.0962	D
$E_2 / E_1 = 4$													
θ_i	$\mathcal{K}_I^{\text{intf}}$	$\mathcal{K}_{II}^{\text{intf}}$	Ψ	$\mathcal{G}_{\text{intf}}$	$\mathcal{K}_I^d$	$\mathcal{K}_{II}^d$	$\mathcal{G}_d$	$\mathcal{R}_1$	$\mathcal{K}_I^p$	$\mathcal{K}_{II}^p$	$\mathcal{G}_p^{\max}$	$\mathcal{R}_2$	Scenario
0°	-3.07E+05	-2.43E+02	0.000	50.0	2.31E+04	-8.88E+04	3.30E+00	0.0661	2.66E+05	-2.31E-02	1.606	0.0161	D
15°	6.28E+05	4.47E+05	0.661	80.2	1.29E+04	-1.03E+05	4.24E+00	0.0529	2.72E+05	3.89E+04	1.867	0.0187	D
30°	6.74E+05	3.70E+05	0.554	69.1	1.10E+04	-1.03E+05	4.19E+00	0.0606	2.71E+05	1.59E+03	1.671	0.0167	D

Table 2 Values of the penetration/deflection parameters for hydro-fracture subjected to bimaterial interface for stiff to soft configuration.

$E_2 / E_1 = 0.5$													
θ_i	$\mathcal{K}_I^{\text{intf}}$	$\mathcal{K}_{II}^{\text{intf}}$	Ψ	$\mathcal{G}_{\text{intf}}$	$\mathcal{K}_I^d$	$\mathcal{K}_{II}^d$	$\mathcal{G}_d$	$\mathcal{R}_1$	$\mathcal{K}_I^p$	$\mathcal{K}_{II}^p$	$\mathcal{G}_p^{\max}$	$\mathcal{R}_2$	Scenario
0°	6.35E+05	-1.36E+02	0.000	50.0	1.16E+04	-1.85E+05	1.62E+01	0.324	1.54E+06	-1.94E+00	215.74	2.157	P
15°	7.04E+05	1.07E+06	1.001	172	3.90E+04	-1.76E+05	1.53E+01	0.0891	1.50E+06	2.23E+05	211.20	2.112	P
30°	4.80E+05	-1.08E+06	-	326	3.79E+04	-1.88E+05	1.74E+01	0.0534	1.57E+06	1.02E+05	223.82	2.238	P
$E_2 / E_1 = 0.25$													
θ_i	$\mathcal{K}_I^{\text{intf}}$	$\mathcal{K}_{II}^{\text{intf}}$	Ψ	$\mathcal{G}_{\text{intf}}$	$\mathcal{K}_I^d$	$\mathcal{K}_{II}^d$	$\mathcal{G}_d$	$\mathcal{R}_1$	$\mathcal{K}_I^p$	$\mathcal{K}_{II}^p$	$\mathcal{G}_p^{\max}$	$\mathcal{R}_2$	Scenario
0°	1.35E+06	-88.83	0.000	50.0	23.38	-3.90E+05	5.96E+01	1.190	4.10E+06	-6.87E+00	1532.62	15.32	P
15°	7.62E+05	4.89E+05	0.590	72.4	4.11E+04	-3.69E+05	5.41E+01	0.748	4.06E+06	1.10E+06	1611.97	16.12	P
30°	3.48E+05	9.55E+05	1.245	487	7.79E+04	-3.99E+05	6.49E+01	0.133	3.56E+06	2.97E+06	1991.44	19.91	P

[2] Khoei, A.R., Vahab, M. and Hirmand, M. An enriched–FEM technique for numerical simulation of interacting discontinuities in naturally fractured porous media. *Comput.Methods in Appl.Mech.Eng.* (2018) **331**:197-231.
[3] Samimi, S. and Pak, A. A fully coupled element-free Galerkin model for hydro-mechanical analysis of advancement of fluid-driven fractures in porous media. *Int. J. Numer. Anal. Methods Geomech*. (2016) **40**:2178-206.
[4] Khoei, A.R. and Bahmani, B. Application of an enriched FEM technique in thermo-mechanical contact problems. *Comput. Mech.* (2018) 1-28.
[5] Geertsma, J. and De Klerk, F. A rapid method of predicting width and extent of hydraulically induced fractures. *J. Petrol. Tech.* (1969) **21**:1571-1581.
[6] Spence, D. and Sharp, P. Self-similar solutions for elastohydrodynamic cavity flow. Proceedings of the Royal Society of London A: Mathematical, Physical and Engineering Sciences: *The. Royal. Society.* (1985) 289-313.
[7] Khristianovic, S. and Zheltov, Y. Formation of vertical fractures by means of highly viscous fluids. *Proc 4th world petroleum congress, Rome* (1955) 579-586.
[8] Hubbert, M.K. and Willis, D.G. Mechanics of hydraulic fracturing. *AIME Pet. Trans.* (1957) **210**:153-168.
[9] Daneshy, A. Numerical solution of sand transport in hydraulic fracturing. *J. Petrol. Tech.* (1978) **30**:132-140.
[10] Haimson, B. and Fairhurst, C. Initiation and extension of hydraulic fractures in rocks. *SPE J.* (1967) **7**:310-318.
[11] Beach, A. Numerical models of hydraulic fracturing and the interpretation of syntectonic veins. *J. Struct. Geo*. (1980) **2**:425-438.
[12] Boone, T.J. and Ingraffea, A.R. A numerical procedure for simulation of hydraulically-driven fracture propagation in poroelastic media. *Int. J. Numer. Anal. Methods. Geomech*. (1990) **14**:27-47.
[13] Secchi, S. and Schrefler, B. A method for 3-D hydraulic fracturing simulation. *Int. J. Fracture.* (2012) **178**:245-258.
[14] Noorishad, J., Tsang, C. and Witherspoon, P. Coupled thermal-hydraulic-mechanical phenomena in saturated fractured porous rocks: Numerical approach. *J. Geophys. Res. B: Solid. Earth.* (1984) **89**:10365-73.
[15] Segura, J. and Carol, I. Coupled HM analysis using zero-thickness interface elements with double nodes. Part I: Theoretical model. *Int. J. Numer. Anal. Methods Geomech*. (2008) **32**:2083-2101.
[16] Réthoré, J., de Borst, R. and Abellan, M.A. A two-scale approach for fluid flow in fractured porous media. *Int. J. Numer. Meth. Eng.* (2007) **71**:780-800.
[17] Khoei, A.R., Vahab, M., Haghighat, E. and Moallemi, S. A mesh-independent finite element formulation for modeling crack growth in saturated porous media based on an enriched-FEM technique. *Int. J. Fracture.* (2014) **188**:79-108.
[18] Vahab, M. and Khalili, N. X-FEM Modeling of Multizone Hydraulic Fracturing Treatments Within Saturated Porous Media. *Rock Mec. Rock. Eng.* (2018) 1-21.
[19] Vahab, M. and Khalili, N. An X-FEM Formulation for the Optimized Graded Proppant Injection into Hydro-fractures Within Saturated Porous Media. *Transp. Porous Media.* (2018) **121**:289-314.

[20] Oliaei, M.N., Pak, A. and Soga, K. A coupled hydro-mechanical analysis for prediction of hydraulic fracture propagation in saturated porous media using EFG mesh-less method. *Comput. Geotech.* (2014) **55**:254-266.
[21] Thiercelin, M., Roegiers, J., Boone, T. and Ingraffea, A. An investigation of the material parameters that govern the behavior of fractures approaching rock interfaces. *6th ISRM Congress* (1987).
[22] Van Eekelen, H. Hydraulic fracture geometry: fracture containment in layered formations. *SPE J.* (1982) **22**:341-349.
[23] Biot, M.A., Medlin, W. and Masse, L. Fracture penetration through an interface. *SPE J.* (1983) **23**:857-869.
[24] Gudmundsson, A. and Brenner, S.L. How hydrofractures become arrested. *Terra Nova.* (2001) **13**:456-462.
[25] Wang, H. Numerical modeling of non-planar hydraulic fracture propagation in brittle and ductile rocks using XFEM with cohesive zone method. *J. Pet. Sci. Eng.* (2015) **135**:127-40.
[26] Behnia, M., Goshtasbi, K., Marji, M.F. and Golshani, A. Numerical simulation of crack propagation in layered formations. *Arab. J. Geosci.* (2014) **7**:2729-2737.
[27] Ming-Yuan, H. and Hutchinson, J.W. Crack deflection at an interface between dissimilar elastic materials. *Int. J. Solids. Struct.* (1989) **25**:1053-1067.
[28] Hutchinson, J.W. and Suo, Z. Mixed mode cracking in layered materials. *Adv. Appl. Mech.* (1991) **29**:63-191.
[29] Akhondzadeh, Sh., Khoei, A.R. and Broumand, P. An efficient enrichment strategy for modeling stress singularities in isotropic composite materials with X-FEM technique. *Engng. Fract. Mech.* (2017) **169**:201-25.
[30] Carter, R. Derivation of the general equation for estimating the extent of the fractured area. Appendix I of "Optimum Fluid Characteristics for Fracture Extension," Drilling and Production Practice, GC Howard and CR Fast, New York, New York, USA, *American Petroleum Institute.* (1957) 261-269.
[31] Witherspoon, P.A., Wang, J., Iwai, K. and Gale, J. Validity of cubic law for fluid flow in a deformable rock fracture. *Water. Resour. Res.* (1980) **16**:1016-1024.
[32] Bouhala, L., Shao, Q., Koutsawa, Y., Younes, A., Núñez, P., Makradi, A. and Belouettar, S. An XFEM crack-tip enrichment for a crack terminating at a bi-material interface. *Engng. Fract. Mech.* (2013) **102**:51-64.
[33] Vahab, M. and Khalili, N. Numerical investigation of the flow regimes through hydraulic fractures using the X-FEM technique. *Engng. Fract. Mech.* (2017) **169**:146-162.
[34] Martínez, D. and Gupta, V. Energy criterion for crack deflection at an interface between two orthotropic media. Journal of the Mechanics and Physics of Solids. 1994;42:1247-71.
[35] Banks-Sills, L., Ashkenazi, D. A note on fracture criteria for interface fracture. *Int. J. Fracture*. 2000;103:177-88.
[36] Vahab, M., Akhondzadeh, Sh., Khoei, A.R. and Khalili, N. An X-FEM investigation of hydro-fracture evolution in naturally-layered domains. *Engng. Fract. Mech.* 2018;191:187-204.